Published in final edited form as:
Nat Struct Mol Biol. 2019 June 19; 26(7): 649–658. doi:10.1038/s41594-019-0256-4.

Multisite phosphorylation code of CDK

Mihkel Örd, **Kaidi Möll**, **Alissa Agerova**, **Rait Kivi**, **Ilona Faustova**, **Rainis Venta**, **Ervin Valk**, and **Mart Loog**
Institute of Technology, University of Tartu, Estonia

Abstract

The quantitative model of cyclin-dependent kinase (CDK) function states that cyclins temporally order cell cycle events at different CDK activity levels, or thresholds. The model lacks a mechanistic explanation, as it is not understood how different thresholds are encoded into substrates. We show that a multisite phosphorylation code governs the phosphorylation of CDK targets and that phosphorylation clusters act as timing tags that trigger specific events at different CDK thresholds. Using phospho-degradable CDK threshold sensors with rationally encoded phosphorylation patterns, we were able to predictably program thresholds over the entire range of the *Saccharomyces cerevisiae* cell cycle. We defined three levels of CDK multisite phosphorylation encoding: (i) Ser-Thr swapping in phosphorylation sites, (ii) patterning of phosphorylation sites, and (iii) cyclin-specific docking combined with modulation of CDK activity. Thus, CDK can signal via hundreds of differentially encoded targets at precise times to provide a temporally ordered phosphorylation pattern required for cell division.

Introduction

Cyclin-dependent kinases (CDKs), the master regulators of cell division, are activated by different cyclins at different cell cycle stages. Despite extensive studies, we do not have a comprehensive answer to the question of how CDKs control the temporal order of cell cycle events. It is not understood how execution timing is encoded into the hundreds of targets to ensure a flawless cell cycle progression. The main obstacle has been combinatorial complexity, because the majority of CDK targets contain intricate patterns of phosphorylation sites, docking sites, and phospho-epitopes[1–5].

*Corresponding author: Mart Loog (mart.loog@ut.ee).
Present address: Institute of Technology, Nooruse 1, Tartu, 50411, Estonia

Data availability
Source data for Figures 1g, i-k, 2a, b, d-h, 3b-h, 4a, c, d, h, i, 5a-c, 6b, c and Supplementary Figures 2a, c-f, 3b, c, 4a-q, 5a-c, e, h, 6a-f are available online. All other data are available upon request.

Author contributions
M.Ö and M.L directed the study. M.Ö, K.M, A.A, R.V and I.F cloned the constructs and made the strains. M.Ö, R.K and E.V purified the proteins. M.Ö performed the microscopy and *in vitro* kinase experiments, M.Ö, K.M and A.A performed the western blotting. M.Ö and M.L wrote the manuscript.

Competing interests statement
The authors declare no competing interests.

Europe PMC Funders Author Manuscripts

The quantitative model proposed by Nurse and Stern, and later experimentally supported by a single cyclin-CDK fusion in fission yeast[6,7], states that cyclin accumulation in the cell cycle leads to rising CDK activity, reaching different activity thresholds necessary for phosphorylation of specific targets[6–9] (Fig. 1a). It has been found that the phosphorylation rate of early substrates is higher compared to late substrates and that efficient phosphorylation of some early targets is dependent on cyclin-substrate interactions[8,10]. However, it is still an open question how CDK can trigger different events at different times, and we do not understand the role of different cyclins in the context of multisite phosphorylation networks.

Three main interactions drive CDK-dependent phosphorylation[11] (Fig. 1b-d). First, the CDK active site recognizes minimal (S/TP) or full consensus motifs (S/TPxK/R)[12,13]. Second, cyclins can bind to specific substrates via linear motifs for substrate targeting[10,14–18]. Third, the Cks1 subunit of the CDK complex interacts with phosphorylated TP sites and directs multisite phosphorylation[4,19,20].

Also, cyclins modulate the intrinsic activity of CDK, with the early G1- and S-cyclins conferring lower activity to Cdk1 than the late G2- and M-cyclins[10,17]. This could function as a mechanism that prevents premature phosphorylation of late targets, while cyclin-specific docking enables weaker G1- and S-CDKs to phosphorylate early targets[8,11,21].

Our goal was to determine if there is a general set of rules, termed the multisite phosphorylation code of CDK, that is used to define CDK thresholds and the execution timing of cell cycle events. The majority of phosphorylation networks are located in intrinsically disordered regions of CDK targets potentially enabling linear encoding of sequence motifs along the primary structure of the protein[1]. Previously, we found that the distances (number of amino acids) between phosphorylation sites and docking motifs may be crucial for CDK thresholds[4,19]. The cyclin-CDK-Cks1 complex could serve as a scaffold for the disordered substrate, mediating an ordered phosphorylation process. According to our hypothesis, the linear motifs (phosphorylation and docking sites) and their patterns function as a barcode, giving a unique identity to each substrate. The cyclin-CDK-Cks1 complex can read the barcode and assign the execution of any CDK-triggered switch to a specified time-point during the cell cycle.

To gain systematic understanding of threshold encoding, we took an approach which stems from the synthetic biology concept of “build to understand”. Using differentially encoded fluorescent threshold sensors in budding yeast, we demonstrate how multisite phosphorylation patterns can be encoded to achieve different CDK thresholds, and thus, different cell cycle timing of specific phosphorylation events. Furthermore, we define a core principle of how the CDK oscillator is separated from the bulk activities of other proline-directed kinases. We show how a CDK activity filter of this type is built using a concept of the “helper network” that only CDK can use.

Results

CDK thresholds can be assigned to proteins by combining linear motifs

We aimed to design substrates that would function as CDK threshold sensors with predictable execution timing over the entire cell cycle. We used non-inhibitory Sic1(1-215)[22], an intrinsically disordered CDK model substrate, as a chassis with phosphorylation-dependent degradation as an output signal for CDK activity. The Sic1 N-terminus contains 8 CDK phosphorylation sites and cyclin docking motifs (LP and 2 RxL motifs)[17] (Fig. 1c). Importantly, the regions between these motifs are highly variable even within the *Saccharomyces* clade (Supplementary Note 1). This suggests that the regions between the motifs function mainly as a linker sequence to achieve the necessary distances between the motifs. First, we aimed to focus on the elements specific for the Cdk1-Cks1 module and excluded the cyclin docking by mutating the RxL and LP motifs (WT sensor) (Fig. 1c)[17]. Using a live-cell fluorescent microscopy protocol we followed the timing of phosphorylation-dependent degradation of GFP-tagged sensors (Fig. 1e). The degradation was measured relative to *Start*, the point when 50% of the G1 transcriptional repressor Whi5 has exited the nucleus (Fig. 1f, Suppl. Fig. 1a, b)[23]. Ubiquitination of Sic1 is mediated by constitutively active SCF-Cdc4[24,25]; therefore the degradation profiles are dependent solely on phosphorylation.

Phosphorylation of two di-phosphodegrons in Sic1 (sites T45-T48 and S76-S80) are a crucial requirement for Sic1 degradation (Fig. 1c)[19,26]. Importantly, site T48 of the first degron does not bear the CDK consensus motif (to be discussed in sections below). To confirm the importance of the degrons as outputs, we analyzed strains that express double mutants of the degrons (Fig. 1g). Degradation was severely reduced, reaching barely the half-maximum levels by the end of mitosis, around 60-80 minutes from *Start*. These two di-phosphodegrons were fixed as the output sites when varying the patterns of motifs in the sensors throughout the study.

Because the distance between the Cks1 priming sites and the degrons is potentially a crucial parameter for degron phosphorylation[4], we first tested the effect of increasing the distance between the priming site T33 and the degron T45-T48 by introducing linkers that were 4 and 8 amino acids long (Fig. 1h). The construct with the wild-type distance of 12 amino acids was degraded at 29 min after *Start*, while the constructs with an extra 4 and 8 amino acids were degraded much later, at 67 and 79 minutes, respectively (Fig. 1i-k). Next, in order to entirely disrupt the Cks1-mediated phosphorylation of the degron, we replaced the threonines with serines in positions 2, 5 and 33, because Cks1 only binds phospho-threonines (Fig. 1c, h)[4,20]. Strikingly, the threshold for this sensor was shifted above the CDK peak as we observed less than 50% degradation during mitosis (Fig. 1i). These experiments confirm that both the optimal distances and Cks1 play crucial roles in threshold encoding.

Next, we showed that it is possible to bring the thresholds down, by adding back the S-CDK-specific RxL docking motifs, confirming that cyclin-specific motifs can be crucial for the earlier thresholds (Fig. 1h-k) and agreeing with results from fission yeast that show that cyclin specificity enhances phosphorylation of ~50% of G1/S targets[8]. These results

highlight an important principle in threshold encoding: the non-optimal phosphorylation clusters that encode higher thresholds can be compensated by cyclin docking to bring the thresholds down. The effects of different barcodes on the phosphorylation dynamics of selected sensors were also verified using Phos-tag western blotting (Suppl. Fig 1c, Supplementary Note 2).

Binary coding of CDK thresholds by serine-threonine swapping

There is potential for rational binary encoding of thresholds by swapping threonines and serines in phosphorylation sites without changing the linear structure of the barcode, while providing 2^N of serine-threonine (S-T) combinations. Different combinations can encode different thresholds via at least two mechanisms. First, the phospho-docking module Cks1 exclusively binds phospho-threonines and not phospho-serines[4,20], therefore the N-terminally positioned threonine sites would lower the thresholds. In contrast, when serines occur in N-terminal positions, the priming mechanism would be lost and the thresholds raised. In addition, by using a kinase assay with peptides that contain CDK consensus motifs, we found that CDK has about 2-3 times higher specificity (k_{cat}/K_M) towards the SP-peptide compared to the TP-peptide (Fig. 2a). This suggests that threonine residues could be phosphorylated later due to differences in CDK specificity. With respect to threshold encoding, it is important that the relative effect of pTP vs pSP with respect to Cks1 docking is much more prominent compared to the active site specificity of S-T, as exemplified using a peptide with a phosphorylated priming site and a secondary site (Fig. 2b).

To explore the possibility of binary coding, we used serine-threonine swapping in threshold sensors with a fixed pattern containing only minimal consensus sites (including T48+1P, which in wild-type Sic1 is a non-consensus site without +1P), and no cyclin docking sites. The degradation of a substrate in which all 8 N-terminal phosphorylation sites were serines (8SP) occurred 27 minutes after *Start* (Fig. 2c-e, Suppl. Fig. 2a). Next, we predicted that when the C-terminal serines (S69-S76-S80) were replaced with threonines (5SP-3TP), the threshold would be shifted up. Indeed, the degradation was delayed for 12 minutes, likely because the sites T69-T76-T80 were less phosphorylated due to the CDK active site serine preference. Because they are located at the C-terminal end of the cluster, they cannot contribute via Cks1 (Fig. 2c-e).

When the sites towards the N-terminus, 45-48, were also mutated to threonines (3SP-5TP), then instead of shifting the threshold further up, a down-shift was observed, leading to degradation only 6 minutes later than the 8SP sensor (Fig. 2c-e). In fact, this result could be predicted if the effect of both Cks1-pTP and CDK active site-SP specificity would be considered. The S-T swapping at sites 45 and 48 creates a docking site for Cks1 and this would compensate for the loss of specificity of the threonine sites.

Next, we tested a sensor that contains the wild-type Sic1 site combination (5TP-3SP), which, unlike the true wild-type, had only minimal consensus sites (Fig. 2c). This construct yielded a threshold that occurred over 20 minutes earlier than the construct 5SP-3TP with the opposite S-T distribution (Fig. 2c-e). Thus, a potentiating effect from the N-terminal Cks1 docking sites combined with favorable active site specificity of the C-terminal serines is superior to the other combinations analyzed above. All threonine construct (8TP) and

3TP-5SP are both degraded relatively early, showing that the effect of C-terminal threonines is lessened in the presence of Cks1 priming sites (Fig. 2c-e, Supplementary Note 3). Additionally, we compared the phosphorylation and degradation of 5SP-3TP and 5TP-3SP sensors with western blot, where a similar 20-minute delay was detected (Suppl. Fig. 2b). Importantly, no accumulation of fully phosphorylated forms could be detected in either case, indicating that the fully phosphorylated forms are rapidly degraded in both serine- and threonine-based degrons (Supplementary Note 4).

Further, we mutated the degron S76-S80 to T76-S80, so that S80 would have preferential specificity compared to T76. The 6SP-1TP-1SP construct, strikingly, was degraded faster than 8SP, which would seemingly contradict the S-T swapping rules (Fig. 2f-h, Suppl. Fig. 2c). However, the N-terminal site of di-phosphodegrons with 3 amino acid mid-distances can be phosphorylated by GSK-3 (Mck1 in budding yeast), which uses the phosphorylated C-terminal site as a primer (Fig. 2i), as demonstrated with Eco1 and Cdc6[27,28]. This could lead to GSK-mediated phosphorylation of T76. To test this hypothesis, we deleted the *MCK1* in these strains and found that the degradation of the 6SP-1TP-1SP sensor was delayed by over 20 minutes (Fig. 2f-g).

The principle of integrating the Mck1 signal was also demonstrated by a sensor where an optimal specificity determinant +3K was added to S80 (6SP-1TP-1SP+3K). This construct was degraded very early (Fig. 2f, h), close to the wild-type sensor with cyclin docking sites (WT+RXL) and 3 optimal CDK motifs (Fig. 1j). This sensor also showed a relatively strong *MCK1* deletion effect compared to the 8SP version. On the other hand, the sensor with wild-type phosphorylation sites showed either no or only a mild delay in a *mck1* background, indicating that when 76-80 degron receives strong Cks1-mediated support, the Mck1 input will have a relatively minor influence. The sensor 3TP-5SP with intermediate Cks1 support for 76-80, shows intermediate effect of Mck1 deletion.

Phosphatase $PP2A^{Cdc55}$ has been shown to preferentially dephosphorylate threonines[29] and could additionally contribute to binary encoding (Supplementary Note 5, Suppl. Fig. 2d-f). Taken together, we demonstrated how substrates with differences only in S-T distribution can have very different phosphorylation dynamics. When the binary encoding is combined with the distance-encoding, one would potentially be able to cover the entire span of cell cycle thresholds with very high temporal resolution.

Cyclin-specific docking motifs in CDK threshold encoding

Our latest studies have revealed that besides the RxL motifs specific for S-CDK[10,14,15,17] (Fig. 1c), the other three major CDK complexes (Cln2-, Clb3-, Clb2-Cdk1, denoted as G1, G2, M complexes) in budding yeast also use specific substrate docking motifs[16,17,30]. This suggests that the entire span of thresholds can be controlled by cyclin-specific mechanisms. We first set out to test the effect of a Cln2-specific docking motif LP[16,17,31]. The degradation of the wild-type sensor was shifted about 10 min earlier by the addition of an LP motif (Fig. 3a-b, e). However, the effect of LP docking was less pronounced when the specificity of the T45-T48 degron was augmented by adding a proline next to T48 (T48+1P, creating a CDK consensus site). Also, a fast single di-phosphodegron (LL**TP**PR**SP**, a modified Cyclin E degron[32,33]) showed less enhancing effect from LP docking. The high affinity

phosphodegron has also been shown previously to lower the threshold for Sic1 degradation[33,34]. These observations introduce an important principle that poor specificity of output site can be compensated by docking. On the other hand, when output sites have high specificity for CDK, the effect of docking is less pronounced.

We have recently discovered an M-CDK-specific motif, LxF, that can strongly potentiate phosphorylation by Clb2-Cdk1[30]. We introduced this motif into sensors where the thresholds had been shifted up by reducing Cks1-dependent phosphorylation of the degrons to target the time window of M-CDK accumulation (Fig. 3a). Strikingly, this motif shifted the thresholds down by 25 35 minutes (Fig. 3c, f).

Recently, we have also mapped a G2-CDK-specific docking motif PxF (Kõivomägi, Kivi, Puss, Örd, Loog, manuscript in preparation). The motif shifted the threshold of T33(+4) sensor by about 15 minutes, which is considerably less than that induced by the M-CDK motif (Fig. 3c-d, f-g). By following the levels of cyclins with fluorescent tags (Fig. 3h, Suppl. Fig. 3a-c) we found that although Clb3 peaked between S-cyclin Clb5 and M-cyclin Clb2[35], it showed a much lower nuclear abundance. This result explains why the M-CDK motif was able to shift the threshold more than the G2-CDK motif. Importantly, we also confirmed that cyclin-specific docking of Clbs acted via the hydrophobic patch, because corresponding mutations in the cyclin pockets (*hpm*) shifted the thresholds back and showed prominent effects *in vitro* (Suppl. Fig. 4a-q, Fig. 3i-j). Therefore, it is possible to encode the CDK thresholds by discriminating even between closely related B-type cyclins using cyclin-specific docking, and the resulting thresholds correlate well with the accumulation timing and abundances of cyclins (for cytoplasmic CDK activity see Supplementary Note 6 and Suppl. Fig. 5). Also, the *in vitro* experiments are consistent with the *in vivo* degradation profiles, which is important evidence that the *in vitro* CDK specificity can be used to predict the thresholds *in vivo*.

Cyclin rearrangements change the order of thresholds

To obtain a full understanding of cyclin specificity in phosphorylation ordering, we replaced the S-cyclin gene *CLB5* at its locus with the M-cyclin gene *CLB2*[36,37] (Fig. 4a). Because the Cdk1 inhibitory kinase Swe1 has higher specificity towards M-CDK[37,38], we also deleted the *SWE1* gene to obtain a direct comparison of M- and S-CDK activities. In the resulting *clb5::CLB2* strain, a threshold sensor with the M-CDK-specific motif (*clb5::CLB2* T33(+4) LxF) showed an impressive 40 minutes earlier degradation compared to the strain with the wild-type cyclin order expressing a construct without docking sites (Fig. 4b-d). Compared to the wild-type strain expressing the sensor with the docking site (T33(+4) LxF), the shift was over 20 minutes. This clearly illustrates that expression of cyclins is correlated with the phosphorylation of specific targets, and that cyclin rearrangement will change the order of thresholds due to cyclin-specific phosphorylation.

Furthermore, in the *clb5::CLB2* strain, the substrate without cyclin docking sites was degraded about 25 minutes earlier, revealing that M-CDK has higher docking independent intrinsic activity, compared to S-CDK (Fig. 4c-d). This result presents *in vivo* evidence for the increasing intrinsic activity principle proposed by us earlier (Fig. 4e-f)[10,17]. Additionally, the sensor bearing the S-CDK motif RxL did not change its threshold upon cyclin

replacement, providing further evidence of this principle, because *in vitro* data predicted that M-CDK, while having only minor specificity for the RxL, can compensate the loss of docking by its higher intrinsic activity[10,17]. This also explains the previously published result that Clb2 can compensate the loss of Clb5 in the clb5::CLB2 swe1Δ strain[37]. Furthermore, targeting specifically M-CDK activity to a late sensor triggers an earlier degradation compared to S-CDK, providing additional evidence for the higher intrinsic activity of M-CDK (Suppl. Fig 6a-b, Supplementary Note 7).

Increasing CDK activity profile is also important to gain better resolution for higher thresholds. If a uniform CDK activity is accumulating, the fold-change in the activity is considerably reduced at higher cyclin levels compared with the early cell cycle. For example, in a simplified cell cycle model where 4 cyclins are expressed sequentially at 10 units each (Fig. 4g), a sharp increase in CDK activity occurs in the early stages of cell cycle. However, in the final stages (progression from 0.75 to 1), only a slight increase of 1.25 times occurs (Fig. 4g). Logarithmically increasing intrinsic activity, however, helps to keep the fold-change, and thus, also the threshold resolution, high during the entire cell cycle (Fig. 4h-i). To illustrate the importance of this quality, we modelled the phosphorylation of 4 substrates with different CDK specificities[39]. Using the simplified cell cycle model (Fig. 4g), we analyzed the phosphorylation of the substrates with CDK activity increasing according to the uniform or logarithmic model. In case of the uniform model, the early substrates are phosphorylated in a switch-like manner, but the substrates with lower kinase specificity are phosphorylated to a much lower extent and have no temporal switch-like resolution (Fig. 4h). However, with CDK activity increasing logarithmically, each substrate is phosphorylated rapidly at the expression of subsequent cyclins (Fig. 4i).

Non-consensus CDK sites as specificity filters: separating CDK from the other proline-directed kinases

The C-terminal site of the T45-T48 degron, the S^{48}TTKS, is a non-consensus CDK site, without the necessary +1P[19]. We hypothesized that a non-proline site could be a filter to prevent other proline-directed kinases from triggering Sic1 degradation. Most of the kinome can be divided into basophilic, acidophilic and proline-directed kinases with relatively overlapping site-specificity[40], which poses an unsolved enigma of how signaling specificity is achieved. According to our hypothesis, although the S/TP sites may have overlapping specificity with other kinases, the non-proline site acts as a filter that transmits only the CDK signal due to the unique Cks1-mediated phosphorylation.

To test this, we measured the levels of the threshold sensors during pheromone treatment, which leads to activation of MAPK Fus3 and inhibition of Cdk1 activity[41,42]. Like CDKs, MAPKs are proline-directed kinases. However, Fus3 and CDK have diametrically opposed signaling functions. While CDK activity leads to the cell cycle, Fus3 activity causes cell cycle arrest in G1 and induces the alternative cell fate program, mating. The system of two opposing kinase signaling pathways has been considered as the most basic model system in cellular decision making between proliferation and differentiation. Paradoxically, however, the opposing decisions are signaled via kinases with overlapping site-specificity.

In pheromone treated cells, Whi5 was localized to the nucleus, which indicates cell cycle arrest in G1 (Fig. 5a). During a two-hour period of the arrest, the levels of wild-type sensor remained stable, and displayed only a mild decrease. However, a construct with an added proline after T48 (T48+1P) was steadily degraded in arrested cells, leading to the loss of over half of the protein during this period (Fig. 5b). This result confirms that when Cdk1 is inhibited, other proline-directed kinases can phosphorylate the S/TP-based di-phosphodegrons but are unable to phosphorylate the degron containing a non-proline site. This non-proline site alone would represent a very high threshold for any proline-directed kinase, which would even exceed the peak value of CDK activity. Adding different "helper networks" of priming and cyclin docking sites will make it possible to encode any threshold downwards, for CDK exclusively.

The filter principle and the number of phosphorylation sites

To demonstrate the importance of the filter principle on the CDK multisite phosphorylation, we designed a substrate construct in which all 8 N-terminal CDK sites of Sic1, including the non-proline site T48, were changed to minimal consensus SP sites (8SP, also used in Fig. 2d). As expected, this substrate was also leaking during pheromone arrest (Fig. 5c). Surprisingly, however, in cycling cells the 8SP substrate was degraded with the same kinetics as the WT substrate (with a non-CDK output site), despite the lack of Cks1-priming sites (Fig. 6a, b).

These results shape an important mechanistic principle of the CDK control system. According to the initial models, the main emerging property of multisite phosphorylation is the ultrasensitivity of the switch (high Hill coefficient) based on distributive-accumulative multisite phosphorylation[33,43]. According to this view, a substrate with 8 minimal consensus sites and at least a 4-site output signal (two di-phosphodegrons) should, in theory, create a very high kinase threshold[39,44]. However, it is still phosphorylated and degraded relatively early in the cell cycle. In addition, with respect to the degradation timing or duration, there is no difference if there are 4, 5 or 8 SP sites (Fig. 6b, Suppl. Fig. 6c-e, Supplementary Note 8). Thus, even the threshold set by a network phosphorylated via non-processive accumulation of phosphates at minimal consensus sites, with no helper docking mechanisms, is relatively low, at about 25 min from *Start*. When one also considers the maturation time of the fluorophores, this corresponds to roughly 25-50% of total cyclin accumulation (Fig. 6c). Furthermore, the degradation starts already at 15 minutes after *Start*, when the cyclin levels are very low meaning that such a substrate is also very vulnerable to integrating signals from other proline-directed kinases in G1 (e.g. Fus3), leading to an undesirable situation where opposing programs, proliferation and differentiation, would be simultaneously activated.

Separation of CDK and other proline-directed kinase signals can be achieved via the use of non-proline CDK sites (see the prediction of such sites among the CDK targets: Supplementary Table 1, 2), and other less accessible sites. Poor accessibility, potentially due to the proximity of the site to a structured domain, however, is quite specific to any protein and cannot be systematically defined. Nevertheless, these sites can be categorized as poorly accessible sites, together with the non-consensus sites, because they need the helper network

to be phosphorylated by CDK. Such sites, when standing alone without the helper network, have a high and unsurpassable threshold for both CDK and the G1 kinases that prevent cell cycle entry (Fus3, Hog1, Kss1, Mpk1, etc.). Addition of a helper network of linear motifs that can be used by CDK, due to its unique docking mechanisms, but not by the other kinases, makes it possible to create a range of CDK thresholds that cover the entire span of the cell cycle (Fig. 6 c, d).

Discussion

This study outlines a principle of how patterns of phosphorylation sites and cyclin docking motifs facilitate encoding of CDK thresholds. Such linear encoding of the timing tags presents a flexible solution for evolutionary tuning of hundreds of thresholds. Although the execution of the CDK-driven switches depends on several factors, such as the affinities of the downstream proteins and conformational changes[2,3], the core principle of processing the kinase inputs of different strength into a certain phosphorylation level provides a mechanistic basis for the CDK quantitative model. Our data clearly show that there can be many distinct thresholds, providing fine-grained control over the order of events from a small number of CDK complexes (Fig. 6c, Suppl. Fig. 6f). Most CDK targets contain multiple phosphorylation sites clustered in disordered regions[1]. The serine-threonine distribution in phosphorylation sites and the pattern of these sites, combined with positioning of cyclin docking motifs creates a unique barcode on each substrate (Suppl. Fig. 6g). Based on the CDK multisite phosphorylation parameters, different Cks1-mediated and cyclin-dependent connections can be predicted for each target (Suppl. Fig. 6g). As shown here, these connections can determine the phosphorylation dynamics of different targets. Importantly, we have shown that there is a high correlation between the *in vitro* phosphorylation specificities and *in vivo* phosphorylation timings in case of the Sic1-based substrates. In addition, there is significant *in vitro* evidence of the impact of Cks1 and cyclin docking on phosphorylation of several CDK targets[4,14,16,17,20,30,31], suggesting that the multisite phosphorylation code is relevant for the temporal ordering of CDK phosphorylation in general. However, depending on the substrate and especially the nature of the output phosphorylation sites, the multisite phosphorylation parameters and the linker regions between the motifs can have different importance in determining the phosphorylation timing.

A striking feature of the CDK multisite phosphorylation code is the possibility of binary coding by serine-threonine swapping. At least three different mechanisms, when combined, can encode a wide range of thresholds without changing the overall pattern of the network. The number of serine-threonine combinations increase with the number of sites in the network (2^N), presenting a simple way to tune cell cycle progression during evolution. In fact, two mechanisms of the binary coding - Cdk1 active site serine preference and threonine specificity of PP2A – have also been observed in metazoans[13,45].

The main principle of encoding the CDK thresholds over the span of the cell cycle is based on the concept of limiting phosphorylation steps that are crucial for output signals. The limiting step in threshold sensors used in this study was the non-consensus site T48 in a di-phosphodegron. In principle, such limiting site can also be poorly accessible due to

structural constraints. However, the relative importance of non-consensus sites as limiting steps in the CDK targets seems to be wide, as more experimental evidence supports the previously unappreciated fact that a large fraction of CDK signaling could be transmitted via non-consensus sites[13,19,46]. Studies by us and Suzuki *et al* indicate that besides the absence of +1P, the other less critical CDK consensus site requirements, +3K/R and -2P[13,17], are often present in non-consensus motifs, which provides a minimal degree of CDK specificity, and distinguishes the sites from random serines and threonines. With the rate-limiting site alone being above the scale of the thresholds, the so called “helper network” becomes the core concept of CDK multisite phosphorylation encoding. These networks, which consist of Cks1 priming sites and cyclin docking modules, can bring the thresholds to any predicted lower level, down to the very early stages of the cell cycle (Fig. 6d).

This study also provides multiple lines of *in vivo* evidence for the logarithmically changing CDK intrinsic activity principle[10,17]. Importantly, besides being a safeguard mechanism to prevent premature triggering of later switches, the logarithmic principle is also important to gain better resolution of the switches at higher thresholds (Fig 4g-i). Additional mechanisms, such as inhibition of CDK or inactivation of phosphatases, also contribute to the modulation of CDK activity during the cell cycle and can improve the resolution of CDK thresholds. While having a lesser role in budding yeast, the Wee1 kinase inhibits the activity of mitotic CDKs in fission yeast prior to mitosis, where the inactivation of Wee1 at mitotic entry creates a sharp increase in CDK activity, necessary for reaching the mitotic thresholds[47–49].

In conclusion, although several proteomics screens and targeted studies on particular CDK-controlled switches have yielded a considerable amount of knowledge of CDK-controlled processes, we still lack a mechanistic understanding of how the most crucial element of the CDK system, the temporal ordering of the hundreds of switches is achieved. There is empirical evidence of CDK thresholds and cyclin specificity, however, it has been difficult to draw a generalized mechanism for threshold encoding because the targets have very different individual structures and downstream functions. In the current study, we took the opposite approach which stems from the synthetic biology concept of “build to understand”. By using a set of threshold sensors, we were able to rationally vary the network parameters and obtain a full set of rules and core mechanistic understanding of the CDK multisite phosphorylation code. Because CDK is not an ordinary kinase with simple ON/OFF switching, but a system operating via multiple thresholds, gaining full control over it as a programmable system would certainly be useful for synthetic biology applications. Even though cells are using the phosphorylation networks ubiquitously, our knowledge has so far been limited for the *de novo* design of synthetic multisite phosphorylation circuits.

Methods

Yeast strains

Yeast strains were MATa haploids of the W303 strain and are described in supplementary table 3. Gene deletions, promoter substitutions and epitope-tagging were performed using standard methods based on PCR-based homologous recombination[50,51]. For C-terminal

tagging with yeCitrine, GFP in pFA6a-GFP-kanMX6[50] was replaced with yeCitrine. The transformants were selected for single-copy integration by fluorescence intensity.

Sic1-based threshold sensors

The threshold sensors were based on a non-inhibitory domain of Sic1 (positions 1-215)[22] and were expressed under native *SIC1* promoter. To restrain the localization of the threshold sensor to either the nucleus or cytoplasm, an SV40 NLS (PKKKRKV) or a NES sequence (NELALKLAGLDINK), respectively, was added to the N-terminus of the protein. In addition, RxL and LP motifs were mutated to reduce the Cln2- and Clb5-specificity of wild-type Sic1[17]. The docking sites were mutated as follows: R13A L15A R89A L91A R114A L116A R147A L149A V136A L137A L138A P139A P140A. In order to increase the ability of Cln2 to fully phosphorylate the sensors, an arginine was introduced to position +2 of phosphorylation sites S69 and S80 (mutations F71R and F82R)[17]. The threshold sensors were C-terminally fused to EGFP via a linker sequence (PGLQEFGAGAGAGAGA).

In thresholds sensors containing RxL motifs, two RxL motifs of Sic1, ^{89}RTLF and ^{114}RILF, were retained as in wild-type protein. In targets with LP motifs, the LP motif in Sic1 ^{136}VLLPP was left unmutated and an additional LP motif from Ste20 (sequence NNVVS**L**DD**PI**Q**F**TRVSS)[16] was introduced to positions 146-162. The PxF and LxF motifs were introduced to the same positions as RxL motifs. In case of PxF motifs, the sequence from Sic1 positions 85-94 and 110-119 was replaced with a PxF motif with sequence PPKG**P**N**F**YAK (Kõivomägi, Kivi, Puss, Örd, Loog, manuscript in preparation). To introduce the LxF motifs, the sequence from Sic1 positions 88-94 and 112-118 was substituted with the sequence PEK**L**Q**F**Y[30].

In threshold sensors where the distance between T33 and T45 was increased by either 4 or 8 amino acids, the sequences PQKP or GQKAPQKP, respectively, were introduced after position 37 in Sic1.

The targets that contained 8 minimal consensus motifs as phosphorylation sites carried the RxL and LP motif mutations as described above and the full consensus motifs in Sic1 (T5, T33 and S76) were mutated to minimal consensus motifs with the following substitutions: R8A, K36A, R79A. In addition, the non-S/TP site ^{48}TT was replaced with the sequence ASP.

The sensor carrying a single optimal di-phosphodegron contained, in addition to the docking site mutations described above, the phosphorylation site mutations (T2A T5A T33A T45A S69A) and the C-terminal degron in positions 74-82 was replaced with the sequence LLTPPRSPR.

Protein purification

Clb5-, Clb3- and Clb2-Cdk1 complexes were purified from yeast cells with the TAP method using C-terminally tagged cyclins as described previously[52,53], except that lysates were prepared using Mixer Mill MM 400 (Retch). For purification of Cln2-Cdk1 complexes, an N-terminally tagged 3HA-Cln2 fusion protein, was overexpressed in yeast cells and purified by immunoaffinity chromatography with antibody against the HA epitope as described[54]

(rabbit polyclonal anti-HA was purchased from Labas, Estonia). Cks1 was purified as described previously[55].

Sic1-based threshold sensors were purified using N-terminal 6His-tag. 6His-tagged proteins were expressed in *E. coli* BL21RP cells at 37 °C using 1 mM IPTG to induce expression. His-tagged proteins were purified using standard cobalt affinity chromatography with 200 mM imidazole used for elution.

Kinase assays

The general composition of the assay mixture contained 50 mM Hepes, pH 7.4, 180 mM NaCl, 5 mM $MgCl_2$, 20 mM imidazole, 2% glycerol, 0.2 mg/ml BSA, 500 nM Cks1 and 500 μM ATP [(with added [γ-32P]-ATP] (Hartmann Analytic). Substrate protein concentrations were 1 μM (in the linear [S] versus v0 range, several-fold below the estimated K_M value). The concentrations of kinase complexes were around 0.2 nM. The kinase assays were performed under conditions below 10% of initial substrate turnover. Reactions were carried out at room temperature and were stopped at two time points (7 and 14 minutes) using SDS-PAGE sample buffer. For separation of differentially phosphorylated forms of the substrate proteins, we used 10% SDS-PAGE supplemented with 100 μM Phos-tag reagent (Wako Pure Chemical Industries). Electrophoresis of Phos-tag SDS-PAGE gels was carried out at 15 mA for 3 hours. For histone H1 peptide kinetics, the peptides with sequences PKTPKKAKKL and PKSPKKAKKL (Inbio) were phosphorylated by Clb2-Cdk1 at 8 peptide concentrations ranging from 1 μM to 3000 μM. Histone H1 peptides were bound to phosphocellulose paper and phosphorylation signals were quantified. The biotinylated Sic1(pT33-T45) peptide (biotin-MQGQK(p)TPQKPSQNLVPVTPSTTKSFK) (Storkbio) was used at 6 concentrations ranging from 1 μM to 300 μM and the phosphorylation reactions were pipetted onto SAM2 Biotin Capture Membrane (Promega Corporation). γ-32P phosphorylation signals were detected using an Amersham Typhoon 5 Biomolecular Imager (GE Healthcare Life Sciences). Signals were quantified using ImageQuant TL (Amersham Biosciences) and GraphPad Prism 5.0 was used for data analysis. All kinase assays were performed in at least two replicate experiments. The number of replicates and the quantified signals for each replicate are available in the source data files online.

Time-lapse fluorescence microscopy

Yeast cultures were grown at 30 °C in synthetic complete media lacking uracil with 2% glucose (SC-URA) to OD 0.2-0.6. Cells were pipetted onto 0.8 mm cover glass slips and covered with a 1 mm thick 1.5% agarose pad made with SC. Before the start of the experiment, cells were held on the slide under the agarose pad for 60 min. Imaging was performed at 30 °C using a Zeiss Observer Z1 microscope with a 63X/1.4NA oil immersion objective and an Axiocam 506 mono camera (Zeiss), using 3x3 binning for imaging. The temperature of the agarose pad was held at 30 °C using a Tempcontrol 37-2 digital from PeCon. Images were taken every 3 minutes and imaging sessions were 8h long. Up to 12 positions were imaged in one experiment using an automated stage and ZEN software. Definite Focus was used to keep the cells in focus during the experiment. Strains expressing threshold sensor-EGFP fusion proteins were exposed for 15 ms using a Colibri 470 LED module. Imaging of cyclins fused with yeCitrine was performed using a Colibri 505 LED

module for 500 ms. Whi5-mCherry was imaged using Colibri 540-580 LED module for 750 ms. All Colibri modules were used at 25% power. Image segmentation, cell tracking and quantification of fluorescence signals was performed using MATLAB (The MathWorks, Inc.) as described in [56]. For every threshold sensor, we analyzed data from at least two repeats with different transformants. Only daughter cells were used for analysis and at least 60 cells from each strain were analyzed. The exact number of cells used in the analysis of each strain can be found in Supplementary Table 3 and also from the source data files available online. In figures where mean fluorescence intensities are plotted, the GFP signal intensities were divided by the maximum signal intensity during the 90-minute period for each cell to remove differences that arise from the different protein levels of different threshold sensors.

Western blotting

The threshold sensors with either nuclear localization signal or nuclear export signal and a C-terminal 3HA tag were expressed from a pRS315 vector under the *ADH1* promoter. Cells were grown in synthetic complete media lacking leucine (SC-LEU) with 2% glucose at 30 °C to OD 0.3. Cells were then treated for 2.5 hours with 1 μg/ml α-factor, washed thoroughly and released into fresh SC-LEU medium. 5 ml of cells were centrifuged every 10 minutes and flash-frozen in liquid N_2. Cells were lysed by bead beating in lysis buffer containing urea. Proteins were separated using Phos-tag SDS-PAGE with 50 μM Phos-tag and 8% acrylamide. Blotting of Phos-tag SDS-PAGE gels was performed using a dry system iBlot (Invitrogen). Purified anti-HA.11 epitope tag antibody (1:500) (clone 16B12, Biolegend) and HRP-conjugated anti-mouse antibody (1:7500) from Labas, Estonia were used to detect the 3HA-tagged proteins.

Bioinformatics

The homologs of Sic1 from budding yeasts were found using the ProViz tool[57]. Multiple sequence alignment and the positional conservation scoring was performed using Jalview[58].

SLiMSearch4[59] was used to search for potential non-S/TP phosphorylation sites from the disordered regions of the yeast proteome. The disorder score (IUPRED) cut-off was set at 0.3. We searched for two motifs, based on different non-S/TP consensus motifs[13,19]: TP.{10,30}[ST][^P][KR][KR] and TP.{8,28}Px[ST][^P].{0,1}[KR].

Reporting Summary

Further information on experimental design is available in the Nature Research Reporting Summary linked to this article.

Supplementary Material

Refer to Web version on PubMed Central for supplementary material.

Acknowledgements

We would like to thank D. Morgan, P. Pryciak, D. Kellogg, M. Kõivomägi and J. Skotheim for valuable comments on the manuscript. We thank M. Peter (ETH Zürich) for providing NES-Cdc4 construct and J. Mihhejev for

technical assistance. The work was supported by ERC Consolidator Grant 649124 and Estonian Science Agency grants Nr. IUT2-21 and PRG550 to M.L.

References

1. Holt LJ, et al. Global analysis of Cdk1 substrate phosphorylation sites provides insights into evolution. Science. 2009; 325:1682–6. [PubMed: 19779198]
2. Fisher D, et al. Phosphorylation network dynamics in the control of cell cycle transitions. J Cell Sci. 2012; 125:4703–11. [PubMed: 23223895]
3. Holt LJ. Regulatory modules: Coupling protein stability to phopshoregulation during cell division. FEBS Lett. 2012; 586:2773–2777. [PubMed: 22664379]
4. Kõivomägi M, et al. Multisite phosphorylation networks as signal processors for Cdk1. Nat Struct Mol Biol. 2013; 20:1415–1424. [PubMed: 24186061]
5. Valk E, et al. Multistep phosphorylation systems: tunable components of biological signaling circuits. Mol Biol Cell. 2014; 25:3456–3460. [PubMed: 25368420]
6. Stern B, Nurse P. A quantitative model for the cdc2 control of S phase and mitosis in fission yeast. Trends Genet. 1996; 12:345–50. [PubMed: 8855663]
7. Coudreuse D, Nurse P. Driving the cell cycle with a minimal CDK control network. Nature. 2010; 468:1074–9. [PubMed: 21179163]
8. Swaffer MP, Jones AW, Flynn HR, Snijders AP, Nurse P. CDK Substrate Phosphorylation and Ordering the Cell Cycle. Cell. 2016; 167:1750–1761.e16. [PubMed: 27984725]
9. Oikonomou C, Cross FR. Rising cyclin-CDK levels order cell cycle events. PLoS One. 2011; 6:e20788. [PubMed: 21695202]
10. Loog M, Morgan DO. Cyclin specificity in the phosphorylation of cyclin-dependent kinase substrates. Nature. 2005; 434:104–8. [PubMed: 15744308]
11. Örd M, Loog M. How the cell cycle clock ticks. Mol Biol Cell. 2019; 30:169–172. [PubMed: 30640587]
12. Songyang Z, et al. Use of an oriented peptide library to determine the optimal substrates of protein kinases. Curr Biol. 1994; 4:973–82. [PubMed: 7874496]
13. Suzuki K, et al. Identification of non-Ser/Thr-Pro consensus motifs for Cdk1 and their roles in mitotic regulation of C2H2 zinc finger proteins and Ect2. Sci Rep. 2015; 5:7929. [PubMed: 25604483]
14. Schulman BA, Lindstrom DL, Harlow ED. Substrate recruitment to cyclin-dependent kinase 2 by a multipurpose docking site on cyclin A. Biochemistry. 1998; 95
15. Wilmes GM, et al. Interaction of the S-phase cyclin Clb5 with an RXL docking sequence in the initiator protein Orc6 provides an origin-localized replication control switch. Genes Dev. 2004; 18:981–91. [PubMed: 15105375]
16. Bhaduri S, Pryciak PM. Cyclin-specific docking motifs promote phosphorylation of yeast signaling proteins by G1/S Cdk complexes. Curr Biol. 2011; 21:1615–23. [PubMed: 21945277]
17. Kõivomägi M, et al. Dynamics of Cdk1 Substrate Specificity during the Cell Cycle. Mol Cell. 2011; 42:610–623. [PubMed: 21658602]
18. Archambault V, Buchler NE, Wilmes GM, Jacobson MD, Cross FR. Two-Faced Cyclins with Eyes on the Targets. Cell Cycle. 2005; 4:125–130. [PubMed: 15611618]
19. Kõivomägi M, et al. Cascades of multisite phosphorylation control Sic1 destruction at the onset of S phase. Nature. 2011; 480:128–131. [PubMed: 21993622]
20. McGrath DA, et al. Cks confers specificity to phosphorylation-dependent CDK signaling pathways. Nat Struct Mol Biol. 2013; 20:1407–1414. [PubMed: 24186063]
21. Kõivomägi M, Skotheim JM. Docking Interactions: Cell-Cycle Regulation and Beyond. Curr Biol. 2014; 24:R647–R649. [PubMed: 25050961]
22. Hodge A, Mendenhall M. The cyclin-dependent kinase inhibitory domain of the yeast Sic1 protein is contained within the C-terminal 70 amino acids. Mol Gen Genet. 1999; 262:55–64. [PubMed: 10503536]

23. Doncic A, Falleur-Fettig M, Skotheim JM. Distinct interactions select and maintain a specific cell fate. Mol Cell. 2011; 43:528–39. [PubMed: 21855793]
24. King RW, Deshaies RJ, Peters JM, Kirschner MW. How proteolysis drives the cell cycle. Science. 1996; 274:1652–9. [PubMed: 8939846]
25. Zhou P, Howley PM. Ubiquitination and Degradation of the Substrate Recognition Subunits of SCF Ubiquitin–Protein Ligases. Mol Cell. 1998; 2:571–580. [PubMed: 9844630]
26. Hao B, Oehlmann S, Sowa ME, Harper JW, Pavletich NP. Structure of a Fbw7-Skp1-Cyclin E Complex: Multisite-Phosphorylated Substrate Recognition by SCF Ubiquitin Ligases. Mol Cell. 2007; 26:131–143. [PubMed: 17434132]
27. Lyons NA, et al. Sequential primed kinases create a damage-responsive phosphodegron on Eco1. Nat Struct Mol Biol. 2013; 20:194–201. [PubMed: 23314252]
28. Al-Zain A, Schroeder L, Sheglov A, Ikui AE. Cdc6 degradation requires phosphodegron created by GSK-3 and Cdk1 for SCFCdc4 recognition in Saccharomyces cerevisiae. Mol Biol Cell. 2015; 26:2609–19. [PubMed: 25995377]
29. Godfrey M, et al. PP2ACdc55 Phosphatase Imposes Ordered Cell-Cycle Phosphorylation by Opposing Threonine Phosphorylation. Mol Cell. 2017; 65:393–402.e3. [PubMed: 28132839]
30. Örd M, Venta R, Möll K, Valk E, Loog M. Cyclin-Specific Docking Mechanisms Reveal the Complexity of M-CDK Function in the Cell Cycle. Mol Cell. 2019; 0
31. Bhaduri S, et al. A docking interface in the cyclin Cln2 promotes multi-site phosphorylation of substrates and timely cell-cycle entry. Curr Biol. 2015; 25:316–325. [PubMed: 25619768]
32. Welcker M, et al. Fbw7 dimerization determines the specificity and robustness of substrate degradation. Genes Dev. 2013; 27:2531–6. [PubMed: 24298052]
33. Nash P, et al. Multisite phosphorylation of a CDK inhibitor sets a threshold for the onset of DNA replication. Nature. 2001; 414:514–521. [PubMed: 11734846]
34. Yang X, Lau K-Y, Sevim V, Tang C. Design Principles of the Yeast G1/S Switch. PLoS Biol. 2013; 11:e1001673. [PubMed: 24130459]
35. Cross FR, Archambault V, Miller M, Klovstad M. Testing a mathematical model of the yeast cell cycle. Mol Biol Cell. 2002; 13:52–70. [PubMed: 11809822]
36. Cross FR, Yuste-Rojas M, Gray S, Jacobson MD. Specialization and Targeting of B-Type Cyclins. Mol Cell. 1999; 4:11–19. [PubMed: 10445023]
37. Hu F, Aparicio OM. Swe1 regulation and transcriptional control restrict the activity of mitotic cyclins toward replication proteins in Saccharomyces cerevisiae. Proc Natl Acad Sci U S A. 2005; 102:8910. [PubMed: 15956196]
38. Keaton MA, et al. Differential susceptibility of yeast S and M phase CDK complexes to inhibitory tyrosine phosphorylation. Curr Biol. 2007; 17:1181–9. [PubMed: 17614281]
39. Gunawardena J. Multisite protein phosphorylation makes a good threshold but can be a poor switch. Proc Natl Acad Sci. 2005; 102:14617–14622. [PubMed: 16195377]
40. Miller CJ, Turk BE. Homing in: Mechanisms of Substrate Targeting by Protein Kinases. Trends Biochem Sci. 2018; 43
41. Chang F, Herskowitz I. Identification of a gene necessary for cell cycle arrest by a negative growth factor of yeast: FAR1 is an inhibitor of a G1 cyclin, CLN2. Cell. 1990; 63:999–1011. [PubMed: 2147873]
42. Gartner A, Nasmyth K, Ammerer G. Signal transduction in Saccharomyces cerevisiae requires tyrosine and threonine phosphorylation of FUS3 and KSS1. Genes Dev. 1992; 6:1280–92. [PubMed: 1628831]
43. Ferrell JE. Tripping the switch fantastic: how a protein kinase cascade can convert graded inputs into switch-like outputs. Trends Biochem Sci. 1996; 21:460–466. [PubMed: 9009826]
44. Ferrell JE, Ha SH, Ha SH. Ultrasensitivity part II: multisite phosphorylation, stoichiometric inhibitors, and positive feedback. Trends Biochem Sci. 2014; 39:556–69. [PubMed: 25440716]
45. Hein JB, Hertz EPT, Garvanska DH, Kruse T, Nilsson J. Distinct kinetics of serine and threonine dephosphorylation are essential for mitosis. Nat Cell Biol. 2017; 19:1433–1440. [PubMed: 29084198]
46. Huis In 't Veld PJ, et al. Molecular basis of outer kinetochore assembly on CENP-T. Elife. 2016; 5

47. Gould KL, Nurse P. Tyrosine phosphorylation of the fission yeast cdc2+ protein kinase regulates entry into mitosis. Nature. 1989; 342:39–45. [PubMed: 2682257]

48. Morla AO, Draetta G, Beach D, Wang JYJ. Reversible tyrosine phosphorylation of cdc2: Dephosphorylation accompanies activation during entry into mitosis. Cell. 1989; 58:193–203. [PubMed: 2473839]

49. McNulty JJ, Lew DJ. Swe1p Responds to Cytoskeletal Perturbation, Not Bud Size, in S. cerevisiae. Curr Biol. 2005; 15:2190–2198. [PubMed: 16360682]

50. Longtine MS, et al. Additional modules for versatile and economical PCR-based gene deletion and modification in Saccharomyces cerevisiae. Yeast. 1998; 14:953–961. [PubMed: 9717241]

51. Janke C, et al. A versatile toolbox for PCR-based tagging of yeast genes: new fluorescent proteins, more markers and promoter substitution cassettes. Yeast. 2004; 21:947–962. [PubMed: 15334558]

52. Puig O, et al. The Tandem Affinity Purification (TAP) Method: A General Procedure of Protein Complex Purification. Methods. 2001; 24:218–229. [PubMed: 11403571]

53. Ubersax JA, et al. Targets of the cyclin-dependent kinase Cdk1. Nature. 2003; 425:859–64. [PubMed: 14574415]

54. McCusker D, et al. Cdk1 coordinates cell-surface growth with the cell cycle. Nat Cell Biol. 2007; 9:506–515. [PubMed: 17417630]

55. Reynard GJ, Reynolds W, Verma R, Deshaies RJ. Cks1 is required for G(1) cyclin-cyclin-dependent kinase activity in budding yeast. Mol Cell Biol. 2000; 20:5858–64. [PubMed: 10913169]

56. Doncic A, Eser U, Atay O, Skotheim JM. An algorithm to automate yeast segmentation and tracking. PLoS One. 2013; 8:e57970. [PubMed: 23520484]

57. Jehl P, Manguy J, Shields DC, Higgins DG, Davey NE. ProViz—a web-based visualization tool to investigate the functional and evolutionary features of protein sequences. Nucleic Acids Res. 2016; 44:W11–W15. [PubMed: 27085803]

58. Waterhouse AM, Procter JB, Martin DMA, Clamp M, Barton GJ. Jalview Version 2--a multiple sequence alignment editor and analysis workbench. Bioinformatics. 2009; 25:1189–1191. [PubMed: 19151095]

59. Krystkowiak I, Davey NE. SLiMSearch: a framework for proteome-wide discovery and annotation of functional modules in intrinsically disordered regions. Nucleic Acids Res. 2017; 45:W464–W469. [PubMed: 28387819]

Europe PMC Funders Author Manuscripts

Europe PMC Funders Author Manuscripts

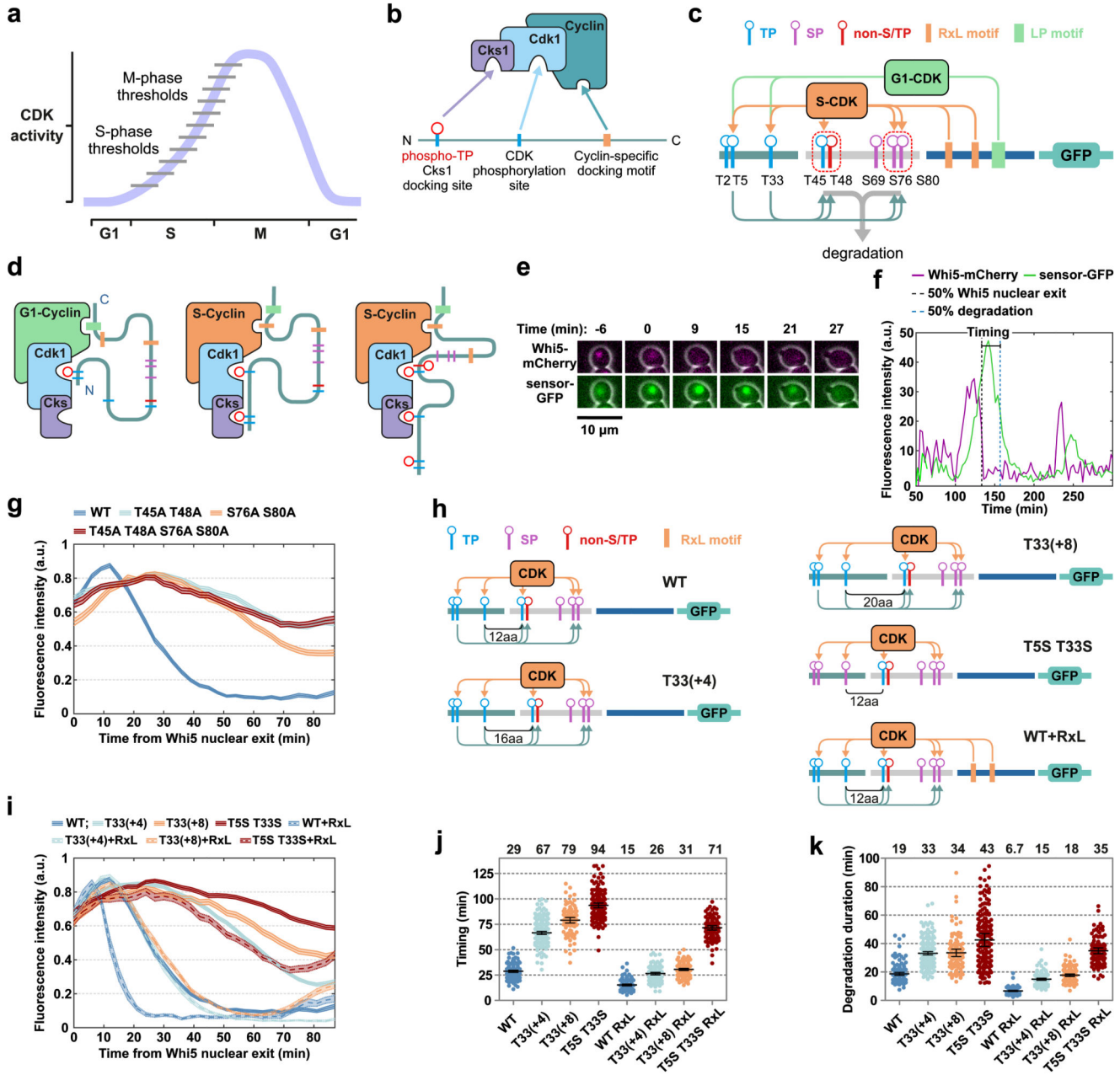

Figure 1. CDK thresholds can be encoded into substrates.

(a) Diagram illustrating the threshold model of CDK function. During late G1, S and early M phase, cyclins accumulate, leading to an increase in CDK activity up to different thresholds. (b) A schematic view of Cdk1-mediated phosphorylation. Three mechanisms determine the phosphorylation rate: the active site specificity, presence of Cks1 binding sites (phospho-TP) and cyclin docking motifs. (c) A scheme showing motifs and docking connections in Sic1 phosphorylation. Three modules in the diagram denote the N-terminal Cks1 docking module (light blue), di-phosphodegron module (grey), and cyclin docking module (dark blue). The arrows below the modules show the Cks1-mediated steps, while the

arrows above designate the cyclin-docking connections. Similar logic is used in the diagrams throughout the study. (d) The dynamics of multisite phosphorylation of Sic1. The N-terminus of Sic1 is shown to take different configurations when binding to the CDK to facilitate the N-to-C-terminal multisite phosphorylation. The rectangular elements denote linear motifs and the circles are the phosphates. Color coding as in panel 'c'. (e) Time-lapse fluorescence microscopy images showing changes in Whi5-mCherry localization and degradation of a threshold sensor fused to EGFP. The time point 0 min marks the 50% nuclear exit of Whi5-mCherry. (f) Quantified nuclear intensities of Whi5-mCherry and sensor-GFP from an exemplary cell over two cell cycles. (g) Plot showing mean nuclear levels of sensors with mutated di-phosphodegrons. The error bars are ±SEM. (h) Schemes depicting the networks of the threshold sensors used in Figure 1i-k. (i) Mean nuclear fluorescence intensities of the indicated threshold sensors with ±SEM error bars. (j-k) Degradation timing and duration in individual cells for the tested threshold sensors. The numbers above the plots show the mean values, the error bars are 95% confidence intervals (CI). Source data for panels g and i-k including information on sample size are available online.

Europe PMC Funders Author Manuscripts

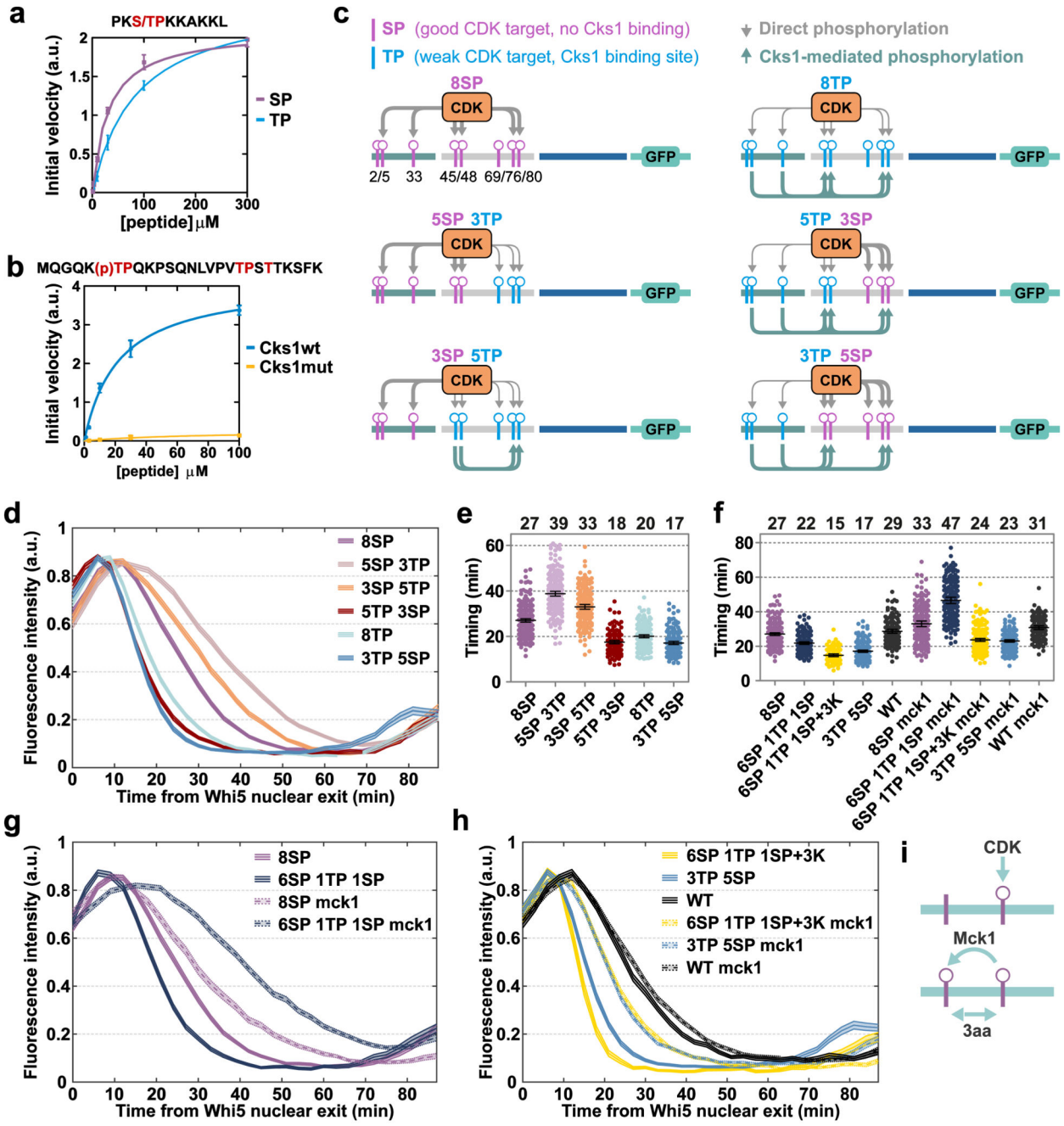

Figure 2. Binary coding of CDK thresholds using S-T swapping.

(a) Steady-state kinetic analysis of the phosphorylation of Histone H1-based model peptide substrates PKTPKKAKKL and PKSPKKAKKL using Clb2-Cdk1-Cks1 complex. (b) Similar kinetic analysis as in 'a' using a primed peptide substrate based on Sic1 containing pT33-T45 using the Clb2-Cdk1 complex with and without Cks1. The plots in panels ‘a’ and ‘b’ show the mean values with standard deviation. Data is from 4 and 2 replicate experiments, respectively. (c) Diagram showing the S/T swapping schemes in the studied threshold sensors. The arrows above the barcode show direct docking-independent

Europe PMC Funders Author Manuscripts

phosphorylation by Cdk1 and the arrows below show Cks1-mediated phosphorylation. The width of the arrows indicates the S/T specificity of CDK and pTP/pSP specificity of Cks1-dependent priming steps. (d) A plot showing the dynamics of threshold sensors with binary S/T codes as indicated on panel 'c'. The graph shows mean of a population of cells, the error bars are ±SEM. (e-f) Plots showing the 50% degradation timing values for individual cells of the indicated sensors in wild-type or mck1 strain backgrounds. The numbers above the plots show the mean value for each sensor and the error bars are 95% CI. (g-h) Plots showing the mean nuclear levels of threshold sensors of the strains presented in 'f'. Error bars are ±SEM. (i) A scheme showing the CDK-primed and Mck1-mediated phosphorylation of a di-phosphodegron. Source data for panels a, b and d-h, including details on sample size are available online.

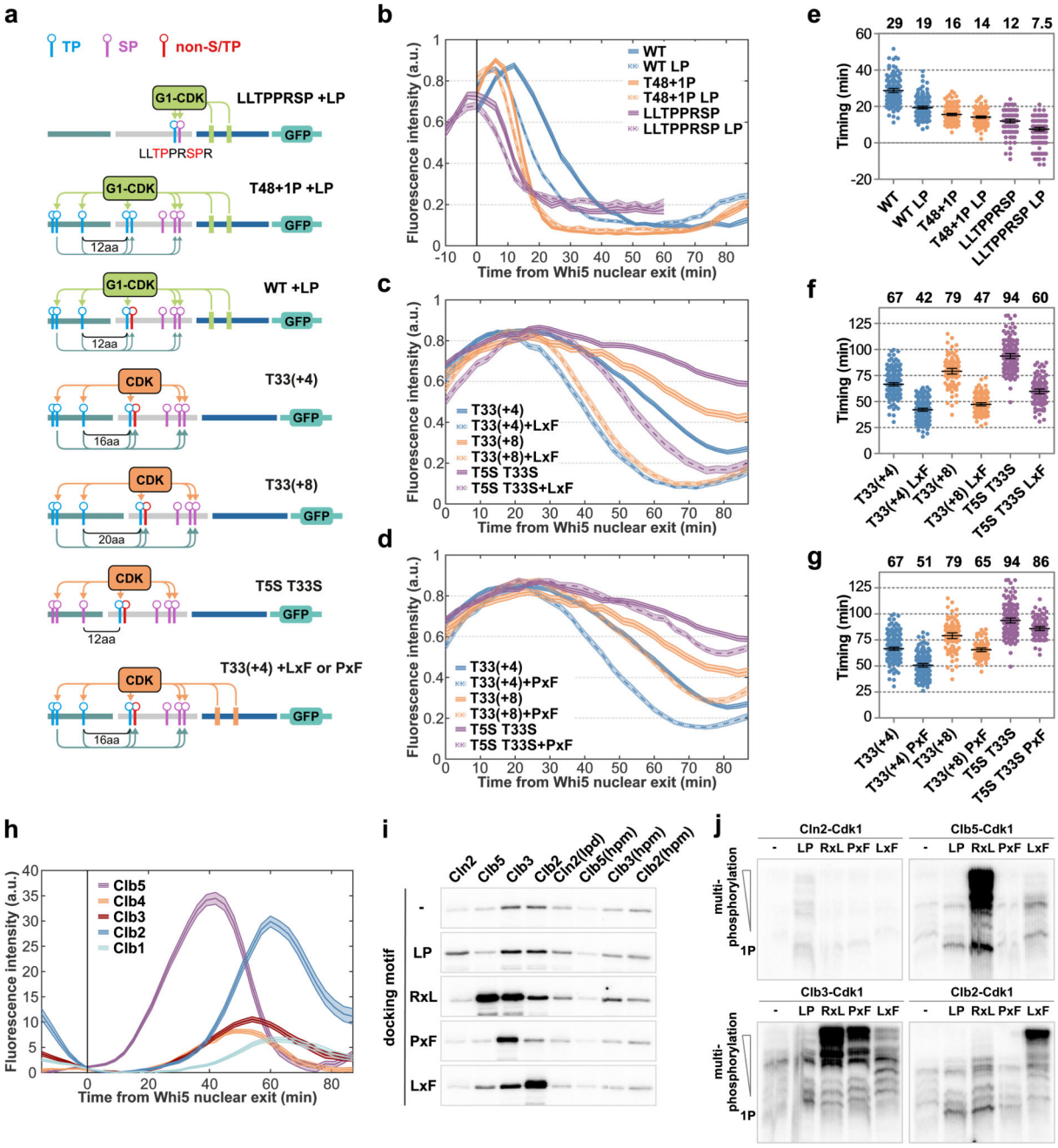

Figure 3. Cyclin-specific encoding of CDK thresholds.

(a) Diagrams of the threshold sensors used in 'b-g'. (b-d) The dynamics of threshold sensors with cyclin specific docking motifs for G1-CDK (LP motif), M-CDK (LxF motif), and G2-CDK (PxF motif). The plots show mean nuclear fluorescence intensities of the sensors ±SEM. (e-g) Plots showing the 50% degradation timing values for individual cells of the strains presented in 'b-d'. The numbers above the plot are the mean values for each strain, the error bars are 95% CI of the mean. (h) Nuclear fluorescence intensities of cyclins fused to Citrine of cells synchronized at the time of 50% of Whi5 nuclear export in late G1. Plot

Europe PMC Funders Author Manuscripts

shows the mean values ±SEM. (i) Autoradiographs showing in vitro phosphorylation of purified threshold sensors with indicated linear docking motif using different wild-type or cyclin-substrate docking mutant CDK complexes (hpm – hydrophobic patch mutant, lpd – LP docking mutant). (j) Similar reactions with wild-type CDK complexes were separated using Phos-tag SDS-PAGE to analyze the multisite phosphorylation pattern. Uncropped gel images are shown in Supplementary Data Set 1. Source data for panels b-h including details on sample size are available online.

Europe PMC Funders Author Manuscripts

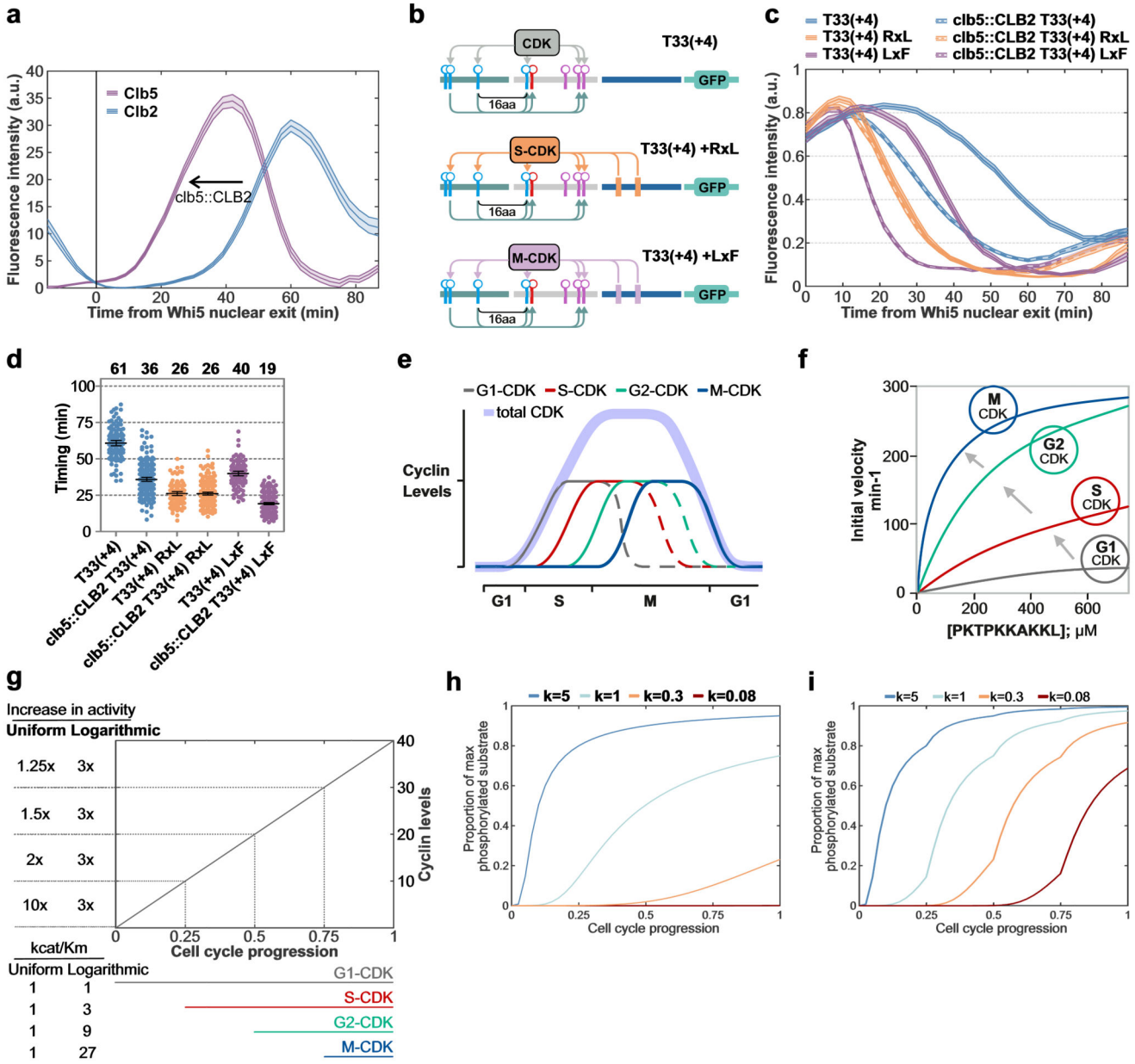

Figure 4. Cyclin rearrangements change the order of the thresholds.

Live-cell microscopy was used to measure the degradation of threshold sensors in swe1Δ and clb5::CLB2 swe1Δ strains. (a) A plot showing the mean ±SEM intensities of S- and M-cyclins (as in Fig. 3h). In clb5::CLB2 strain, CLB2 is placed into CLB5 locus and expressed from CLB5 promoter. (b) Diagrams of the threshold sensors used in 'c,d'. (c) Plot showing mean nuclear levels of the sensors in swe1Δ or clb5::CLB2 swe1Δ strain background. The error bars are ±SEM. (d) Plots showing degradation timing values for the indicated sensors in single cells. The numbers above the plot show the mean for each sensor, the error bars are 95% CI. (e,f) Diagrams showing the principle of changing intrinsic activity of CDK. The phosphorylation specificity of CDK complexes towards a consensus phosphorylation motif rises in the order of expression of cyclins in the cell cycle. 'f' is adapted from Kõivomägi et

Europe PMC Funders Author Manuscripts

Europe PMC Funders Author Manuscripts

al., 2011[17], published under a CC BY license. (g) A diagram illustrating a simplified cell cycle where 4 cyclins are sequentially expressed at equal levels (10 units each). In the uniform model, all cyclins confer identical activity to the CDK, while in the logarithmic model, the activity of subsequent cyclins increases by a factor of 3. “Increase in activity” shows the rise in CDK activity in the period between the dotted lines. (h,i) Steady-state accumulation of maximally phosphorylated substrate with 6 phosphorylation sites with an ordered distributive phosphorylation mechanism was simulated using the formula y = (k*u)6/(1+k*u+(k*u)2+(k*u)3+(k*u)4+(k*u)5+(k*u)6), where k is the rate constant of the kinase divided by the rate constant of phosphatase, and u is the relative concentration of the kinase compared to the phosphatase. In 'h', the CDK activity follows the uniform model, while in 'i' the CDK activity follows the logarithmic model presented in 'g'. Source data for panels a, c, d, h and i, including details on sample size, are available online.

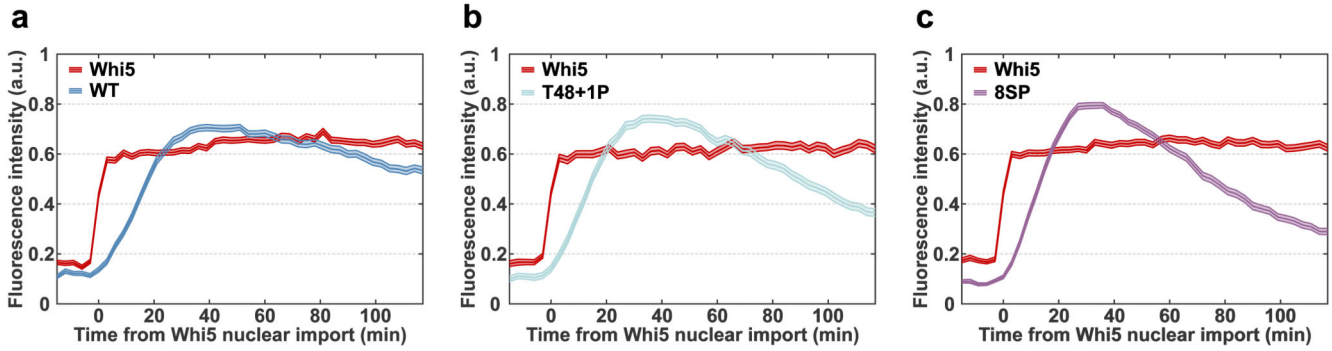

Figure 5. Non-consensus CDK sites as specificity filters: separating the CDK oscillator from the other kinase activities.

(a-c) Levels of the indicated threshold sensors were followed during a two-hour period of pheromone induced G1 arrest using time-lapse fluorescence microscopy. Whi5-mCherry levels are shown in red. Plots show the mean nuclear levels of the sensors. The error bars are ±SEM. Source data for Figure 5 including details on sample size are available online.

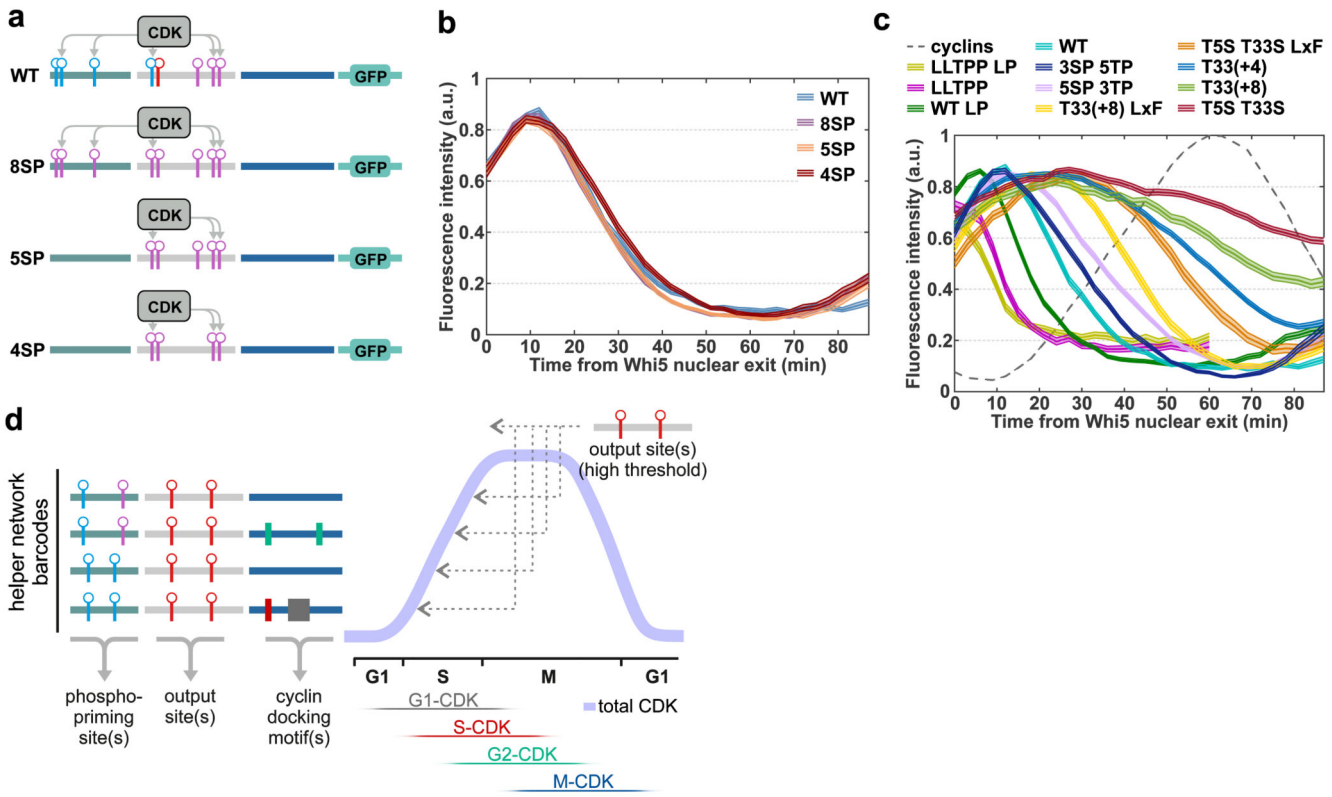

Figure 6. Helper networks in output site phosphorylation and the number of phosphorylation sites.

(a) Diagrams of the threshold sensors with decreasing number of SP sites used in 'b'. (b) Mean intensities of threshold sensors in the cell cycle measured by time-lapse microscopy. The error bars are ±SEM. (c) Mean ±SEM fluorescence intensities of differentially encoded CDK threshold sensors covering the entire span of the cell cycle are plotted relative to Start as t=0 (50% Whi5-mCherry nuclear exit). The accumulation of cyclins is shown as a sum of different cyclin levels from Figure 3h. (d) Diagram illustrating the encoding of thresholds into CDK substrates. Phosphorylation of output sites can be differentially enhanced by various helper networks containing Cks1 binding sites and cyclin docking motifs. Source data for panels b and c including details on sample size are available online.

Europe PMC Funders Author Manuscripts